



Evaluation of Functionally Graded Architecture using Fused Filament Fabrication Technique for Bone Scaffold Applications

Muhammad Azfar Noordin¹, Mohd Aidil Syukri Zulkipli¹, Nur Aqila Kadir Hussein¹, Amir Putra Md Saad^{1,2*}

¹Applied Mechanics and Design, School of Mechanical Engineering, Faculty of Engineering
Universiti Teknologi Malaysia, Johor Bahru, 81200, MALAYSIA

²Medical Devices and Technology Centre (MEDiTEC), Institute of Human Centred and Engineering (iHumEn),
Universiti Teknologi Malaysia, Johor Bahru, 81200, MALAYSIA

*Corresponding Author

DOI: <https://doi.org/10.30880/ijie.2022.14.02.001>

Received 30 April 2021; Accepted 30 September 2021; Available online 02 June 2022

Abstract: Bone scaffold architecture affects the performance of bone scaffold significantly. Recently, functionally graded architecture (FGA) has received wide attention in bone scaffold application due to its architecture that mimics the cancellous bone architecture. Hence, this study aims to evaluate the mechanical properties of PLA specimens that adopt FGA fabricated using additive manufacturing via fused filament fabrication (FFF). The mechanical properties of FGA PLA specimen (1 GPa -2 GPa) was tailored to the cancellous bone (modulus: 0.01 GPa – 2 GPa). The result shows that radially dense- in rod (RDR) has the highest Young's Modulus, and yield strength. However, the relationship between cross section area of specimen needs to be considered in comparing the performance of FGA PLA specimen.

Keywords: Functionally graded architecture, bone scaffold, mechanical properties, polymer

1. Introduction

The human skeleton system has a terrific potential to regenerate itself after injury if the injury size is not critical [1]. The critical size of a bone defect is ranged between 1–3 cm in which implants are needed if the injury is critical [2]. The application for bone scaffold as a bone implant for bone defects has been studied extensively in the past few decades [3–5]. The usual architecture of bone scaffold usually involves only uniform distribution of pore and strut size. However, cancellous bone architecture involves non uniform architecture, in which the thickness and spaces of trabeculae varies depending on the skeletal site. In general, cancellous bone that is situated towards cortical usually has denser trabecular since stress transferred from cortical simulate bone synthesis [6]. Besides, skeletal site of the bone also affects the cancellous bone architecture as different skeletal site expose differently to the stress [7]. Hence, functionally graded architecture (FGA) is the way in moving forward in bone scaffold application. Polymers such as polyethylene terephthalate (PET), poly(lactic-co-glycolic acid) PLGA, (poly ε-caprolactone) PCL, (polyethylene glycol) PEG, (polybutylene terephthalate) PBT, (polylactic acid) PLA and (polyglycolic acid) PGA has been received attention in for implant application [8–11]. In addition to that, PLA has been certified safe by U.S. Food and Drug Administration (FDA) for clinical application which shows good biocompatibility [12], [13]. Despite of that, polymer is considered inferior in terms of mechanical strength in relative to metal, ceramic, and composite [14]. However, PLA has a Young's modulus of (0.3- 4.14 GPa), which is sufficient for possible cancellous bone application [15,16]. There are many studies that used

*Corresponding author: amirputra@utm.my

2022 UTHM Publisher. All rights reserved.

penerbit.uthm.edu.my/ojs/index.php/ijie

PLA as potential material for bone scaffold application. Gregor et al. fabricated a uniform architecture bone scaffold using PLA filament using ordinary commercial 3D printer [8]. Noordin et al. developed a uniform PLA porous scaffold and analyse the mechanical properties of bone scaffold using finite element analysis [3]. Rodrigues et al. manufactured and analysed uniform PLA porous scaffold using FFF in terms of mechanical strength and degradation [17]. However, the above studies do not apply the FGA in developing PLA bone scaffold.

A good bone scaffold should have several characteristics in terms of mechanical properties, permeability, biodegradability and biocompatibility [18]. In terms of mechanical properties, the application of bone scaffold is essential to determine the type of experiment that need to be conducted [19]. Application of bone scaffold on the femur or tibia will need compression experiment as femur and tibia experiences more compression load in relative to other types of due to its nature of skeletal site that support weight bearing. In this study, the bone scaffold is intended for the use in femur reconstruction. Several factors will influence the performance of bone scaffold application such manufacturing technology, material used and scaffold architecture. For example, applying subtractive manufacturing to produce bone scaffold will produce higher mechanical strength in relative to additive manufacturing [20] but subtractive manufacturing has limitation in producing complex architecture such as FGA. Additionally, FGA type of scaffold enables to absorb more energy compared to their uniform counterpart during loading [21]. The bone scaffold architecture is important as it can affect the aforementioned characteristics greatly [22]. Recently, several studies have been made to evaluate the performance of FGA for bone scaffold application [21,23–25]. However, the application of FGA using additive manufacturing via fused filament fabrication, FFF for polymer is very limited. Hence, this paper would highlight and evaluate the use of FFF in FGA using polylactide (PLA) material.

2. Materials and Method

2.1 Manufacturing of Bone Scaffold

Different types of specimens were designed and modelled in CAD software as shown in Fig. 1. The specimens were designed with a bulk volume of 18×18×18 mm. PLA filament was used as the material in the additive manufacturing. A 3D printer machine (Ultimaker 3, Netherlands) with a resolution of 20 micron was used in manufacturing the specimen with 100% infill. The additive manufactured specimens are as shown in Fig. 2 with characteristics as displayed in Table 1. Solid specimen was also being fabricated to act as a control. Three replications were made for each type of specimen.

2.2 Compression Test

Compression test were done by using universal testing machine (Instron 8874, Norwood, USA). The strain rate was set at 1.4 mm/min by using 25kN load cell until the specimens failed. Replications were made and the young's modulus and yield strength were determined using ISO 844 standards.

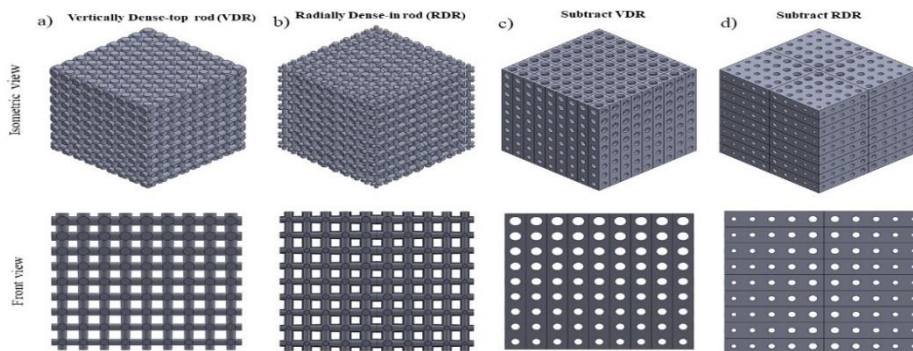


Fig. 1 - 3D model design for PLA specimens

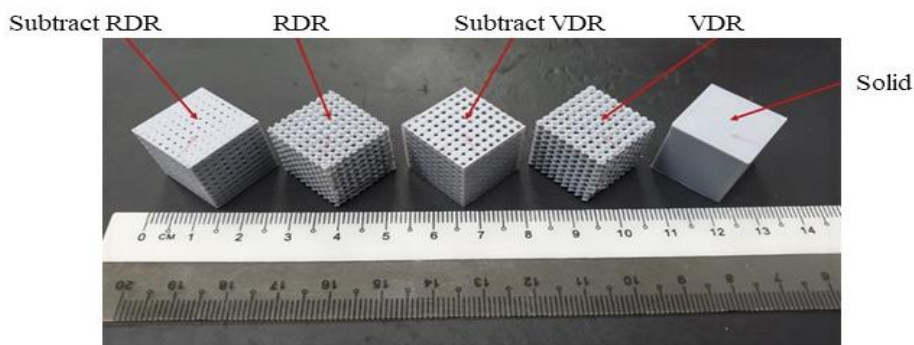


Fig. 2 - PLA specimens

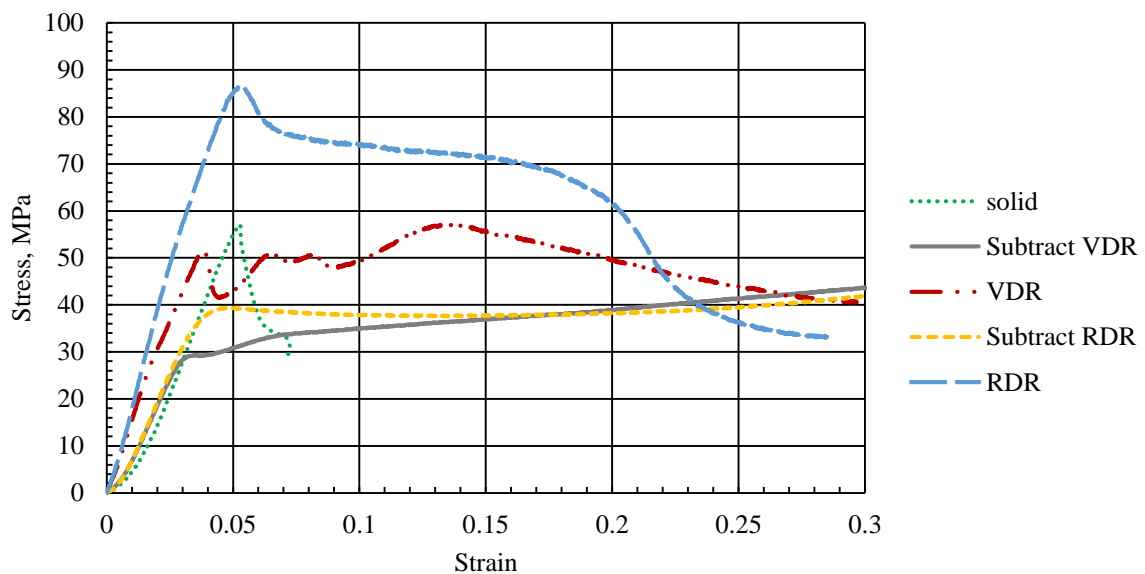
Table 1 - Characteristics of fabricated specimens

Model	Volume (mm ³)	Porosity (%)	Top surface Cross sectional area (mm ²)	Total Surface area (mm ²)
Vertically Dense-top rod (VDR)	5832.0 8	58.70	91.53	25197.60
Radially Dense-in rod (RDR)	5831.4 8	64.83	56.08	7992.36
Subtract VDR (SVDR)	3423.2 1	41.30	232.47	17333.70
Subtract RDR (SRDR)	3780.6 1	35.17	267.92	14749.96
Solid	5832	0	324	1944

3. Result and Discussion

3.1 Stress Strain Curve for Every Sample

In Fig. 3, the stress strain curve of solid and porous PLA specimens under compression test. The straight-line in the early staged of PLA specimens stress- strain curve implies that a linear or direct relationship throughout elastic region, the material obeys the Hooke's law. In addition to that, the PLA specimens exhibits brittle behaviour. This is because, the value of stress of the solid specimen immediately goes down once yield is achieved. For sample SVDR and SRDR, value of stress goes up after the specimens is further compressed is because densification has occurred as the strut of the PLA specimens totally collapsed and the surface of PLA specimen is overlapping to each other. However, for RDR and VDR, densification does not occur due to the rod architecture that prevents the PLA specimen to overlap each other when it is being further compress. In addition to that, it could be observed that the rodlike FGA (RDR and VDR) has superior strain energy density compared to the SVDR and SRDR as both of them has higher surface area of the below stress – strain curve. Moreover, RDR and VDR exhibits anisotropic behaviour in contrast to SRDR and SVDR. This can be shown in Fig. 3, in which the stress- strain curve for RDR and VDR that shows sudden dropped in stress value which indicate plastic collapsed occur. Meanwhile, SRDR show smooth and steady increase in stress and strain value up until 0.3 strain of compression without any sudden drop in stress value.

**Fig. 3 - Stress- strain curve of PLA specimens under compression test**

3.2 Mechanical Properties

Fig. 4 shows the mechanical properties of PLA specimens with the associated cross-section area in terms of Young's modulus, yield strength and stiffness. In general, all of the PLA specimens have a Young's modulus that is in ranged with the cancellous bone (0.01-2 GPa) [26]. It could be deduced that the PLA specimen that has higher young's modulus have higher yield strength too. RDR has the highest modulus and yield strength followed by VDR, solid, SRDR and SVDR. In general, the higher the porosity of a specimen, the lower the mechanical properties of the specimens [20]. This statement could be shown when solid is compared to SRDR and SVDR specimen, in which solid has the highest

mechanical properties followed by SRDR and SVDR respectively. However, in the case of RDR and VDR, both PLA specimen has higher mechanical properties than solid specimen although the solid has lower porosity. This can be due to the lower cross section area of RDR and VDR as $\sigma = F/A$, where σ is stress, F is axial load and A is cross section area. The value of A is inversely proportional to the value of σ which means lower value of A will result of higher stress. This can be further shown in Fig. 4(c) that shows the value of stiffness in N/mm unit in which solid has the highest value followed by, SRDR, SVDR, VDR and RDR. When A is disregarded, the value of stiffness of PLA specimens follows the concept of the lower the porosity, the lower the mechanical properties of the sample. In general, the architecture of scaffold effects the mechanical properties of the scaffold which can be shown by Bartnikowski et al. [27] works, in which in their study that the 90° angle strut design scaffold has the highest mechanical properties in relative with other angle strut design with a significant percentage although the porosity of all the bone scaffold is relatively the same.

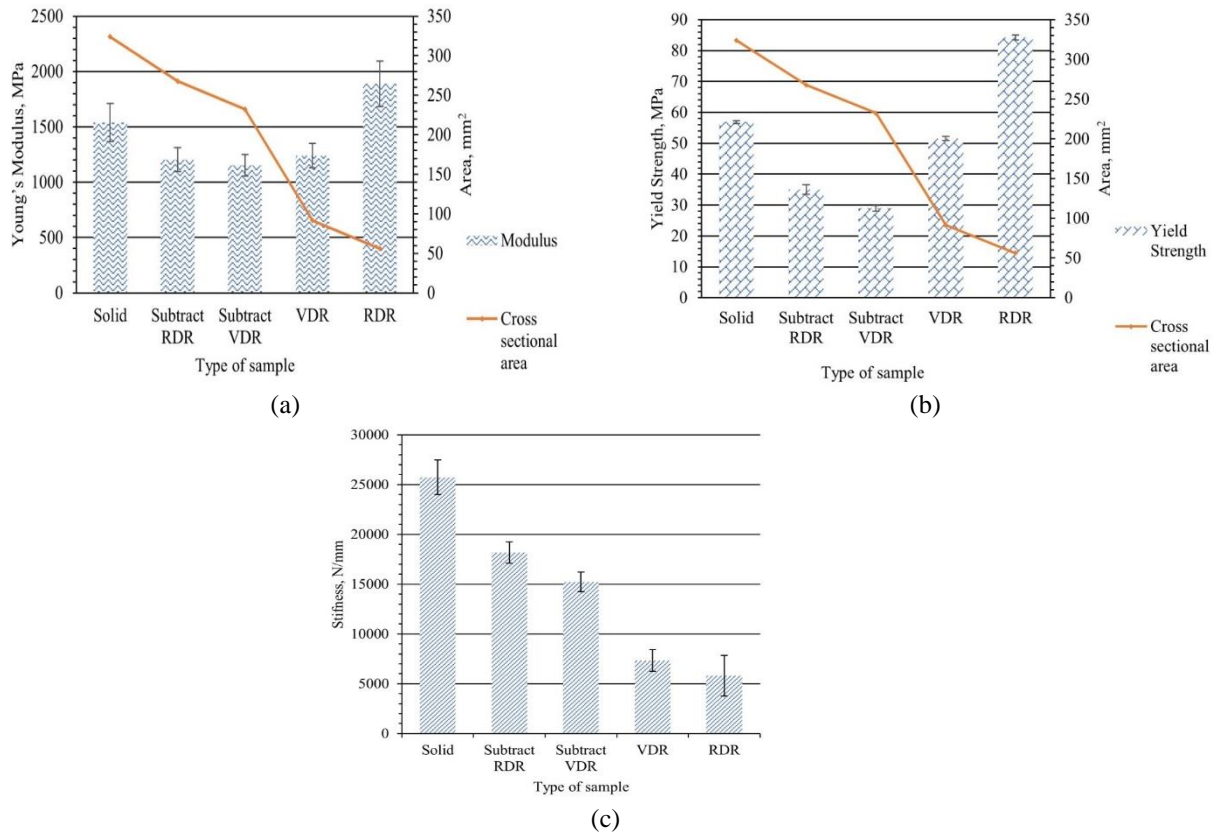


Fig. 4 - Mechanical properties of PLA specimens: a) modulus; b) yield strength; c) stiffness

3.3 Fracture Mechanism

Fig. 5 shows the fracture mechanism of PLA specimens namely SVDR, VDR, SRDR and RDR. Syahrom et al. [28] has classified 3 types of fracture that occurs in cancellous bone during uniaxial compression test namely, oblique fracture, perpendicular global fracture and scattered localized fracture. Solid cube PLA undergoes perpendicular global fracture due to the uniformly 100% infill solid structure. In case of SVDR, as the compression progress, it could be observed that perpendicular fracture take place starting from the upper part of the specimen since SVDR has smaller strut size (higher porosity) at the top part of the specimen. As SVDR is further compressed densification started as the scaffold strut of lower and upper part overlap each other which can be proven in Fig. 3 which indicates the increase of stress value of SVDR when it was being compressed to 0.3 strain. On the other hand, VDR experiences initial perpendicular global fracture at the lower part of the specimen as the VDR has smaller strut size (higher porosity) at the lower part. Densification in VDR only occurs during the initial point (at 0.14 strain) as shown in Fig. 3 and beginning to drop afterwards. However, SRDR responds was a bit different from SVDR and VDR in which the deformity of the specimen occurs uniformly between the upper part and lower part. The global perpendicular fraction occurs at the centre (as marked in Fig 5(c)) of the specimen as the porosity of SRDR varies not in vertically manner but in radial manner. As it is being further compressed, densification could be observed starting to occur in which the specimen is being overlapped in layer form which can be proven in the increasing of stress value of SRDR stress- strain curve in Fig. 3 and Fig. 5(d) shows the behaviour of RDR when it is being compressed uniaxially. It can be observed that RDR fracture mechanism is partially oblique fracture in which fracture initiation occurs at the side upper part and side lower part fracture. This is due to the architecture of RDR which has smaller strut that (higher porosity) at the side of the specimen. When the specimen was being compressed, RDR tend to collapse slantly as oblique fracture occurred and densification did not happen as the RDR

did not overlap with each other as shown in the decrease of stress value of RDR in Fig. 3 after compressive strength was achieved. Although the all the specimens were using the same material, the fracture behaviour of the specimens were different from one another due to different architecture.

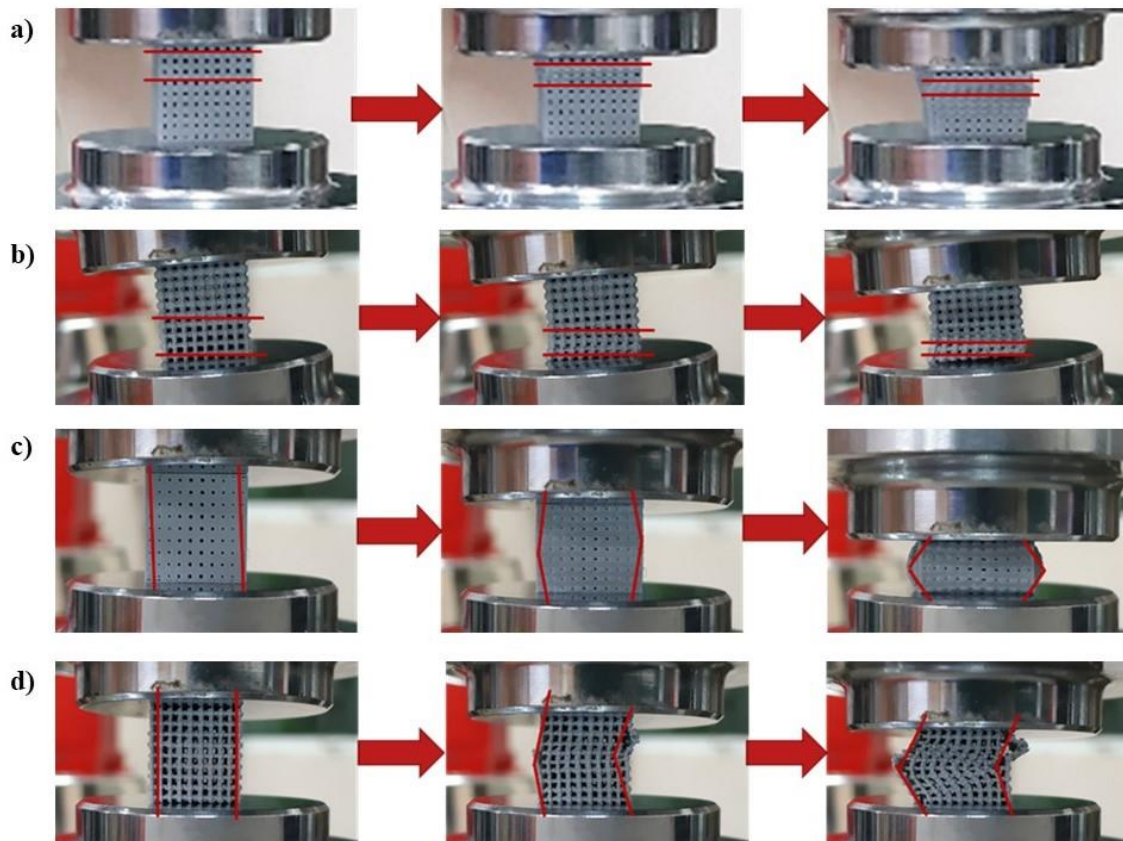


Fig. 5 - Fracture mechanism of: a) SVDR; b) VDR; c) SRDR; d) RDR

4. Conclusion

Polymeric based bone scaffold can be considered as temporary cancellous bone analogue as all of the PLA specimen has modulus ranged from 1 GPa to 2 GPa which is in the range of cancellous bone modulus. In case of mechanical properties, RDR and VDR type of structure exhibits superior mechanical properties in terms of modulus and yield strength in relative to SRDR and VDR. However, RDR and VDR is inferior to SRDR and SVDR in terms of stiffness which means RDR and VDR are less suitable in skeletal site, where high deformities are needed.

Acknowledgement

This project was sponsored by Ministry of Higher Education Malaysia via the Fundamental Research Grant Scheme (FRGS/1/2018/TK03/UTM/02/8). The authors would like to express our deepest gratitude to Research Management Centre in Universiti Teknologi Malaysia (UTM) for managing the project.

References

- [1] Schubert, T., Lafont, S., Beaurin, G., Grisay, G., Behets, C., Gianello, P., & Dufrane, D. (2013). Critical size bone defect reconstruction by an autologous 3D osteogenic-like tissue derived from differentiated adipose MSCs. *Biomaterials*, 34(18), 4428–4438.
- [2] Schemitsch, E. H. (2017). Size matters: Defining critical in bone defect size. *Journal of Orthopaedic Trauma*, 31(5), S20–S22.
- [3] Noordin, M. A., Saad, A. P. M., Ngadiman, N. H. A., Mustafa, N. S., Mohd Yusof, N., & Maaram, A. (2021). Finite element analysis of porosity effects on mechanical properties for tissue engineering scaffold. *Biointerface Research in Applied Chemistry*, 11(2), 8836–8843.
- [4] Ngadiman, N. H. A., Mohd Yusof, N., Idris, A., Misran, E., & Kurniawan, D. (2017). Development of highly porous biodegradable γ -Fe₂O₃/polyvinyl alcohol nanofiber mats using electrospinning process for biomedical application. *Materials Science & Engineering C*, 70, 520–534.
- [5] Kadir, M. R. A., Syahrom, A., & Ochsner, A. (2010). Finite element analysis of idealised unit cell cancellous

- structure based on morphological indices of cancellous bone. *Medical & Biological Engineering & Computing*, 48, 497–505.
- [6] Klein-Nulend, J., Bacabac, R., & Bakker, A. (2012). Mechanical loading and how it affects bone cells: The role of the osteocyte cytoskeleton in maintaining our skeleton. *European Cells and Materials*, 24, 278-291.
- [7] Clarke, B. (2008). Normal bone anatomy and physiology. *Clinical Journal of the American Society of Nephrology*, 3, S131–S139.
- [8] Gregor, A., Filova, E., Novak, M., Kronek, J., Chlup, H., Buzgo, M., Blahnova, V., Lukasova, V., Bartos, M., Necas, A., Hosek, J. (2017). Designing of PLA scaffolds for bone tissue replacement fabricated by ordinary commercial 3D printer. *Journal of Biological Engineering*, 11, 1–21.
- [9] Singh, Y. P., Moses, J. C., Bhunia, B. K., Nandi, S. K., & Mandal, B. B. (2018). Hierarchically structured seamless silk scaffolds for osteochondral interface tissue engineering. *Journal of Materials Chemistry B*, 6, 5671–5688.
- [10] Ghassemi, T., Shahroodi, A., Ebrahimzadeh, M. H., Mousavian, A., & Movaffagh, J. (2018). Current concepts in scaffolding for bone tissue engineering. *The Archives of Bone and Joint Surgery*, 90, 90–99.
- [11] Kashte, S., Sharma, R. K., & Kadam, S. (2020). Layer-by-layer decorated herbal cell compatible scaffolds for bone tissue engineering: A synergistic effect of graphene oxide and *Cissus quadrangularis*. *Journal of Bioactive and Compatible Polymers*, 35, 57–73.
- [12] Qi, F., Wu, J., Li, H., & Ma, G. (2019). Recent research and development of PLGA/PLA microspheres/nanoparticles: A review in scientific and industrial aspects. *Frontiers of Chemical Science and Engineering*, 13, 14–27.
- [13] Milovanovic, S., Markovic, D., Mrakovic, A., Kuska, R., Zizovic, I., Frerich, S., & Ivanovic, J. (2019). Supercritical CO₂ - assisted production of PLA and PLGA foams for controlled thymol release. *Materials Science and Engineering C*, 99, 394–404.
- [14] Mondal, S., & Pal, U. (2019). 3D hydroxyapatite scaffold for bone regeneration and local drug delivery applications. *Journal of Drug Delivery Science and Technology*, 53, 101131–101142.
- [15] Kashirina, A., Yao, Y., Liu, Y., & Leng, J. (2019). Biopolymers as bone substitutes: A review. *Biomaterials Science*, 7, 3961–3983.
- [16] Farah, S., Anderson, D. G., & Langer, R. (2016). Physical and mechanical properties of PLA, and their functions in widespread applications - A comprehensive review. *Advanced Drug Delivery Reviews*, 107, 367–392.
- [17] Rodrigues, N., Benning, M., Ferreira, A. M., Dixon, L., & Dalgarno, K. (2016). Manufacture and Characterisation of Porous PLA Scaffolds. *Procedia CIRP*, 49, 33–38.
- [18] Zhao, H., Li, L., Ding, S., Liu, C., & Ai, J. (2018). Effect of porous structure and pore size on mechanical strength of 3D-printed comby scaffolds. *Materials Letters*, 223, 21–24.
- [19] Burgers, T. A., Mason, J., Niebur, G., & Ploeg, H. L. (2008). Compressive properties of trabecular bone in the distal femur. *Journal of Biomechanics*, 41, 1077–1085.
- [20] Noordin, M. A., Rahim, R. A. A., Roslan, A. N. H., Ali, I. A., Syahrom, A., & Saad, A. P. M. (2020). Controllable macroscopic architecture of subtractive manufactured porous iron for cancellous bone analogue: Computational to experimental validation. *Journal of Bionic Engineering*, 17, 357–369.
- [21] Yu, S., Sun, J., & Bai, J. (2019). Investigation of functionally graded TPMS structures fabricated by additive manufacturing. *Materials & Design*, 182, 108021–10830.
- [22] Li, Y., Jahr, H., Pavanram, P., Bobbert, F. S. L., Puggi, U., Zhang, X. Y., Pouran, B., Leeflang, M. A., Weinans, H., Zhou, J., & Zadpoor, A. A. (2019). Additively manufactured functionally graded biodegradable porous iron. *Acta Biomaterialia*, 96, 646–661.
- [23] Li, D., Liao, W., Dai, N., & Xie, Y. M. (2019). Comparison of mechanical properties and energy absorption of sheet-based and strut-based gyroid cellular structures with graded densities. *Materials*, 12, 2183–2198.
- [24] Zhang, X., Fang, G., Xing, L., Liu, W., & Zhou, J. (2018). Effect of porosity variation strategy on the performance of functionally graded Ti-6Al-4V scaffolds for bone tissue engineering. *Materials & Design*, 157, 523–538.
- [25] Zhang, X. Y., Fang, G., Xing, L. L., Liu, W., & Zhou, J. (2018). Effect of porosity variation strategy on the performance of functionally graded Ti-6Al-4V scaffolds for bone tissue engineering. *Materials and Design*, 157, 523–538.
- [26] Gibson, L. J. (1985). The mechanical behaviour of cancellous bone. *Journal of Biomechanics*, 18, 317–328.
- [27] Bartnikowski, M., Klein, T. J., Melchels, F. P. W., & Woodruff, M. A. (2014). Effects of scaffold architecture on mechanical characteristics and osteoblast response to static and perfusion bioreactor cultures. *Biotechnology and Bioengineering*, 111, 1440–1451.
- [28] Syahrom, A., Abdul Kadir, M. R., Abdullah, J., & Ochsner, A. (2011). Mechanical and microarchitectural analyses of cancellous bone through experiment and computer simulation. *Medical and Biological Engineering and Computing*, 49, 1393–1403.